Journal of Neuroscience Methods 372 (2022) 109537

Contents lists available at ScienceDirect

Journal of Neuroscience Methods

journal homepage: www.elsevier.com/locate/jneumeth

Altered resting fMRI spectral power in data-driven brain networks during development: A longitudinal study

Oktay Agcaoglu [a,*], Tony W. Wilson [b], Yu-Ping Wang [c,d], Julia M. Stephen [e], Zening Fu [a], Vince D. Calhoun [a,e]

[a] Tri-institutional Center for Translational Research in Neuroimaging and Data Science (TReNDS), Georgia State University, Georgia Institute of Technology, Emory University, 55 Park Place, NE, 18th floor, Atlanta, GA 30303, USA
[b] Institute for Human Neuroscience, Boys Town National Research Hospital, 378 Bucher, Boys Town, NE 68010, USA
[c] Department of Biomedical Engineering, Tulane University, 6823 St. Charles Avenue, New Orleans, LA 70118, USA
[d] Department of Global Biostatistics and Data Science, Tulane University, 1440 Canal Street, New Orleans, LA 70112, USA
[e] The Mind Research Network, 1101 Yale Blvd NE, Albuquerque, NM 87106, USA

ARTICLE INFO

Keywords:
Longitudinal analysis - brain development
Resting state - eyes open - eyes closed
Independent component analysis
Amplitude of low frequency fluctuations
Frequency spectrum analysis

ABSTRACT

Background: Longitudinal studies provide a more precise measure of brain development over time, as they focus on within subject variability, as opposed to cross-sectional studies. This is especially important in children, where rapid brain development occurs, and inter-subject variability can be large. Tracking healthy brain development and identifying markers of typical development are also critically important to diagnose mental disorders at early ages.

New method: We track longitudinal changes in spectral power of time-courses using a unique non-binning approach assessed with group independent component analysis, in a large multi time-point resting state functional magnetic resonance imaging dataset (N = 124) containing healthy children from 8.2 to 17.6 years old (m=12.6) called the Developmental Chronnecto-Genomics study. We examined how eyes open (EO) and eyes closed (EC) resting states play a role in age-related spectral differences, as several studies have reported differences in these conditions.

Results: Typical brain development shows increased spectral power in low frequencies and decreased spectral power in high frequencies in as children grow and develop, for both the EO and EC conditions. In addition, we observed significant differences in power spectra between EO and EC and between sexes, mainly suggesting higher spectral power in females at middle and high frequencies. A replication analysis using the Adolescent Brain Cognitive Development data (N = 3371, mean age 9.9 years old) further supported this result, also showing general increases in low frequencies and decreases in higher frequencies, though some network level differences are present comparing to the main dataset.

Comparison with existing method: Our results indicate that spectral power changes significantly with typical development and our non-binning approach shows these changes with more detailed frequency resolution comparing to binning approaches. This is important as many studies reported an association of higher frequency power with brain disorders.

Conclusion: Our findings of decreased spectral power in the high frequencies with development may be a general marker of typical development., though this needs further investigation.

1. Introduction

Frequency domain analysis of functional magnetic resonance imaging (fMRI) data has provided useful insight about brain function. Starting with the initial observation (Biswal et al., 1995) that low frequency fluctuations in resting state-fMRI (rs-fMRI) (<0.1 Hz) can provide an estimate of functional connectivity, there have been several studies on analyzing rs-fMRI data in the amplitude of low frequency

* Corresponding author.
E-mail addresses: oagcaoglu@gsu.edu (O. Agcaoglu), tony.w.wilson@gmail.com (T.W. Wilson), wyp@tulane.edu (Y.-P. Wang), jstephen@mrn.org (J.M. Stephen), zfu@gsu.edu (Z. Fu), vcalhoun@gsu.edu (V.D. Calhoun).

https://doi.org/10.1016/j.jneumeth.2022.109537
Received 24 September 2021; Received in revised form 1 February 2022; Accepted 20 February 2022
Available online 23 February 2022
0165-0270/Published by Elsevier B.V.

fluctuations (ALFF)(Zang et al., 2007) and its altered version of fractional ALFF (fALFF) (Zou et al., 2008). Altered ALFF has been reported in multiple mental and neurological disorders including schizophrenia (Fu et al., 2018; Turner et al., 2013), attention-deficit/hyperactivity disorder; (Wang et al., 2016; Zang et al., 2007), amyotrophic lateral sclerosis, and stroke patients (Egorova et al., 2017). ALFF/fALFF studies have often used seed or region of interest based analysis and are usually focused on the total power between 0.01 Hz and 0.08 Hz. Recently, some studies have used other frequency bands to calculate ALFF/fALFF, such as slow 4: 0.027–0.073 Hz, and/or slow 5: 0.01–0.027 Hz. (Zhan et al., 2016).

Some studies have compared frequency differences in focused frequency bins rather than summing across specific intervals. For example, Garrity et al. (2007) found decreased power in low frequencies and increased power in high frequencies in schizophrenia patients compared to control group in default mode networks. Calhoun et al. (2011) compared the spectral power in group independent component analysis (gICA) time-courses between bipolar patients, schizophrenia patients and control group and found higher power in lower frequencies (0–0.1 Hz) and lower power in higher frequencies (0.01–0.25 Hz) in an auditory oddball task dataset in schizophrenia and bipolar disorder. Allen et al. (2011) reported altered spectral power in the resting state network (RSN) time-courses with age, which also varied in males vs females. Rs-fMRI data were also investigated in a 4D spatial-temporal framework in (Miller et al., 2015) and (Agcaoglu et al., 2016), which found significant differences between patients with schizophrenia and control group in left and right hemispheres.

In the current study, we analyzed the frequency spectrum from 0.01 Hz to 0.15 Hz in a longitudinal dataset of children from ages 8–17 called Developmental Chronnecto-Genomics (Dev-CoG) (Stephen et al., 2021). The purpose of this study is to examine whether there are clearly discernable developmental patterns in the spectra of resting-state fMRI using a non-binning approach. Such patterns could shed light on important markers of normative development, which in the future could be used to identify aberrant developmental trajectories in those with emerging psychiatric and/or neurological conditions. We used a longitudinal approach because there is considerable evidence in the literature that brain development can show non-linear trajectories and inter-subject variability can be very high in these age groups, which may prevent replicable results in cross sectional studies. Thus, in this paper, we utilized a longitudinal dataset and focused on the time-related differences. We hypothesized that the employed method may provide more robust and replicable trajectories of development. To support our hypothesis, we also applied our method to an independent dataset consisting of 3371 subjects from the Adolescent Brain Cognitive Development (ABCD) dataset(Casey et al., 2018). To the best of our knowledge, this is the first study that tracks longitudinal changes of rs-fMRI spectral power in children.

2. Method and materials

2.1. Participants

We utilized the full longitudinal Dev-CoG dataset, which is an extension of the cross-sectional analyses representing the single time point reported previously(Agcaoglu et al., 2019; Agcaoglu et al., 2020). Resting state fMRI scans were collected from children at two different sites (Mind Research Network (MRN)/New Mexico and the University of Nebraska Medical Center (UNMC)/Nebraska) under both EO and EC conditions as part of the National Science Foundation (NSF) supported Dev-CoG project (http://devcog.mrn.org/). The study protocols were approved by the relevant institution review board (IRB) prior to study initiation at each data collection site (Advarra IRB – MRN and UNMC IRB – Nebraska) and the research was carried out in compliance with the Declaration of Helsinki. Participants were recruited at each site from local communities, with the goal of matching the local demographics in racial and ethnic categories. The inclusion criteria were age 9–14 years at enrollment, able to speak English, willing and able to provide assent/consent by both child and parents; the exclusion criteria were being pregnant, unable to provide consent, history or current mental or developmental disorders, history or current epilepsy or other neurological disorders, parental history of major psychiatric or neurological disorders, parent-reported prenatal exposure to alcohol or drugs, medication use indicative of psychiatric or neurological disorder, an individual education plan indicative of a developmental delay/disorder, contraindication to MRI and orthodontia (e.g. braces or spacers). Please see Stephen, Solis et al. (2021) for details of the study. Participants were instructed to close their eyes but remain awake during the EC condition and were asked to stare at a fixation cross during the EO scan. There were 713 scans from 148 subjects with multiple timepoint scans available. We excluded scans having poor registration, low signal to noise ratio (less than 150), or incomplete datasets, resulting in 574 scans from 124 subjects with some participants having more than two timepoints available. In the final analysis, we included 470 EO and EC scans with data from at least two timepoints from 124 participants (age range from 8.2 to 17.6 years). The minimum time between scans for any individuals was 100 days (m=592, std=218), and we selected the two most separated timepoints if multiple timepoints were available. The retained participants had a maximum mean framewise displacement (MFD) of 0.25 mm. For the EO condition, data from 62 males and 58 females were available, and for the EC condition, data from 60 males and 55 females were available. The mean age was 11.81 and 13.48 for the first and second time point respectively. The mean time interval between scans was 584.9 days (standard deviation(std) 221.7 days) in EO case; for the EC case, mean interval was 597.9 days (std= 214.8 days). The average time intervals were 615.7 days (std=219.5 days) and 564.8 days (std=214.1) for males and females respectively. Note that when participants had more than two scans available, we took those with the longest interval between.

We checked to see any significant differences between females and males that could bias the results. There were slightly more male participants than female participants. There wasn't any significant age difference between sexes (1st time point, mean females= 11.87, mean males= 11.75, $p = 0.57$; 2nd time point: mean females=13.30, mean males = 13.66, $p = 0.13$) and scan time interval was slightly higher for males (615 days) comparing to females (564 days); however, two-sample t-test didn't reveal any significant differences($p = 0.0737$).

ABCD study recruited nearly 10,000 youth aged 9–10 years old across the US with the aim to track human brain development from childhood through adolescence. Participants were recruited using a school base strategy and the sample were aimed to resemble US population's sociodemographic status as closely as possible. Scans were collected at 21 different sites in EO condition and were optimized and harmonized. (Casey et al., 2018; Jernigan et al., 2018). We included 3371 subjects whose multi time point spectra results were available; 1552 girls and 1819 boys, mean age at first scan is 9.9 years old (std = 0.6, min = 8.9, max = 11.1) and mean age at second scan is 11.9 years old (std = 0.6, max = 13.4, min = 10.6); longitudinal scan interval has a mean of 1.9 years (std = 0.13, max = 2.6, min = 1.4).

2.2. Imaging parameters

Imaging data were collected on a 3 T Siemens TIM Trio scanner at the MRN site and on a 3 T Siemens Skyra scanner at the Nebraska site. A total of 650 volumes of multiband echo planar imaging blood-oxygen-level-dependent data (a length of 4 min and 59 s) were collected per resting state condition and per participant with repetition time (TR) of 0.46 s, time to echo of 29 ms, flip angle of 44 degrees, and a slice thickness of 3 mm with no gap. Rs-fMRI scans were acquired using a standard gradient-echo planar imaging paradigm; MRN site: field-of-view (FOV) of 246 × 246 mm (82 ×82 matrix), 56 sequential axial slices; Nebraska: FOV of 268 × 268 mm (82 ×82 matrix), 48 sequential

axial slices. Eyes of the participants were monitored via an eye-tracker during the EO condition to ensure that participants were following the instructions. The order of the EO and EC scanning sessions were counterbalanced across participants at both sites.

The ABCD study were collected at 21 different sites, using Siemens Prisma, Phillips and GE 750 3 T scanners with harmonized imaging parameters, in EO condition and passive viewing of a cross hair with a TR of 0.8 s. Please see (Casey et al., 2018) for the details of the ABCD study parameters.

2.3. Preprocessing

The preprocessing of the DevCog data included image distortion corrected using FSL's topup (https://fsl.fmrib.ox.ac.uk/fsl/fslwiki/) and re-alignment to the single-band reference image (SBref) using AFNI's align_epi_anat.py (https://afni.nimh.nih.gov/). Motion parameters were estimated relative to SBref and data was registered to the Montreal Neurological Institute (MNI) template using AFNI's 3dNwarpApply as estimated using AFNI's auto warp.py. The first 4 volumes were excluded to account for the T1 equilibrium effect. The participants consisted of children with an age range of 8.2–17.6 years, therefore we re-warped the data to a study specific template computed as the average of the first time point from each scan. Finally, the data was smoothed to 6 mm full-width at half maximum. The ABCD data were preprocessed using an automated analysis pipeline based in SPM, which included image realignment, slice timing correction, spatially normalizing to MNI space, and smoothing.

2.4. Group independent component analysis

In a previous study (Agcaoglu et al., 2019), a part of this dataset from a single timepoint was decomposed into 150 independent components and 51 components were retained as intrinsic resting networks. The 51 RSNs were labeled and ordered/grouped based on their anatomical and functional properties including 4 sub-cortical networks (SC), 3 auditory networks (Aud), 8 sensorimotor networks (SM), 18 visual networks (Vis), 4 default-mode networks (DMN), 12 cognitive control networks (CC), and 2 cerebellar networks (Cb). In this longitudinal study, we utilized spatially constrained ICA with the selected and ordered components as references. Preprocessed functional data were analyzed with a spatially constrained ICA algorithm, based on multi-objective optimization (MOO-ICAR) (Du et al., 2013) and (Du et al., 2016), implemented in the group ICA of fMRI toolbox (GIFT) software (http://trendscenter.org/software/gift). Using this approach, we estimated scan specific spatial maps (SMs) and time courses (TCs). These RSNs are displayed in Fig. 1 and the corresponding anatomical regions, and their peak locations are detailed in Table 1. Please see Agcaoglu et al. (2019) for additional details of the gICA and RSN selection process.

ABCD data were decomposed into 53 RSN by utilizing a spatially constrained ICA using the spatial maps from the NeuroMark study; and SMs derived from two large-sample healthy control datasets, (Du et al., 2020); and used the available power spectral density estimated using the GIFT software.

2.5. Spectra estimation

After gICA, we further analyzed the subject specific TCs. We

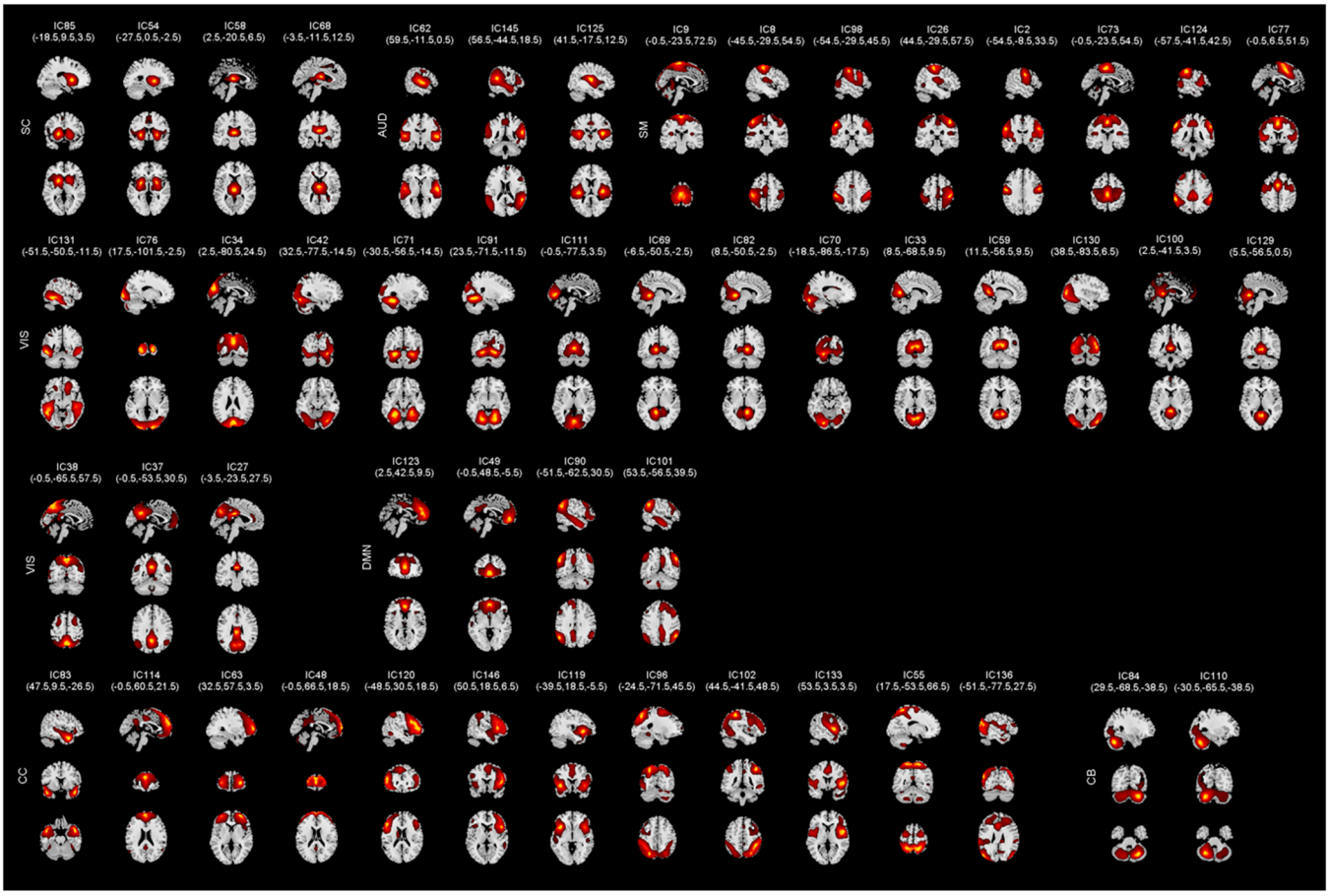

Fig. 1. Fifty-one Resting State Networks; grouped according to their anatomical and functional properties; four SC, 3 Aud, 8 SM, 18 Vis, 4 DMN, 12 CC and 2 Cb (Agcaoglu et al., 2019).

Table 1
Anatomical regions corresponding to each RSN presented in Fig. 1. Number of voxels, maximum t-value, coordinates of the peak and Broadman area number are shown (Agcaoglu et al., 2019).

RSN#	Nv	Tmax	Coord.	BA
Sub-Cortical Networks				
85				
Left Putamen	1463	141.63	-18 10 4	
Right Putamen	735	82.27	20 12 0	
54				
Right Putamen	1224	135.54	26 4 − 2	
Left Putamen	1197	147.24	-28 0 − 2	
58				
Right Thalamus	1033	170.69	2 − 20 6	
68				
Left Thalamus	1430	141.33	-4 − 12 12	
Auditory Networks				
62				
Left Superior Temporal Gyrus	2267	84.25	-52 − 18 6	22
Right Superior Temporal Gyrus	2029	87.45	60 − 12 0	22
145				
Right Superior Temporal Gyrus	3713	104.6	56 − 44 18	13
Left Middle Temporal Gyrus	1378	51.41	-58 − 54 12	22
125				
Right Insula Lobe	1908	119.75	42 − 18 12	13
Left Superior Temporal Gyrus	1795	107.6	-46 − 24 12	41
Sensorimotor Networks				
9				
Left Paracentral Lobule	2599	94.33	0 − 24 72	6
8				
Left Postcentral Gyrus	1828	94.76	-46 − 30 54	2
Right Postcentral Gyrus	383	37.47	54 − 20 48	1
98				
Left Inferior Parietal Lobule	2438	96.03	-54 − 30 46	2
Right SupraMarginal Gyrus	1621	76.73	60 − 20 40	3
26				
Right Postcentral Gyrus	2515	96.98	44 − 30 58	2
Left Postcentral Gyrus	507	37.30	-42 − 38 60	40
2				
Left Postcentral Gyrus	1080	91.31	-54 − 8 34	6
Right Postcentral Gyrus	1014	90.70	60 − 6 30	6
73				
Left Paracentral Lobule	4219	125.8	0 − 24 54	6
Left Rolandic Operculum	157	40.96	-40 − 26 18	13
124				
Left Inferior Parietal Lobule	1073	76.71	-58 − 42 42	40
Right SupraMarginal Gyrus	873	73.92	60 − 38 40	40
77				
Left SMA	4587	101.23	0 6 52	6
Right Insula Lobe	516	53.27	48 10 − 2	22
Visual Networks				
131				
Left Inferior Temporal Gyrus	2183	74.55	-52 − 50 − 12	37
Right Fusiform Gyrus	1668	60.82	44 − 30 − 18	20
76				
Right Calcarine Gyrus	2756	81.86	18 − 102 − 2	18
34				
Left Cuneus	3412	82.78	2 − 80 24	18
42				
Right Fusiform Gyrus	1510	72.64	32 − 78 − 14	19
Left Cerebellum	569	36.52	-40 − 68 − 20	19
71				
Left Fusiform Gyrus	1920	77.93	-30 − 56 − 14	19
Right Fusiform Gyrus	1422	69.95	30 − 48 − 18	37
91				
Right Lingual Gyrus	4008	91.16	24 − 72 − 12	19
111				
Left Lingual Gyrus	2891	109.15	0 − 78 4	18
69				
Left Cerebellum	1662	143.19	-6 − 50 − 2	30
82				
Right Cerebellum	1674	142.59	8 − 50 − 2	30
70				
Left Lingual Gyrus	2152	76.07	-18 − 86 − 18	18
33				
Right Calcarine Gyrus	3313	115.61	8 − 68 10	30
59				
Right Lingual Gyrus	2465	127.29	12 − 56 10	30
Left Middle Occipital Gyrus	293	41.29	-42 − 80 30	19
RSN#	Nv	Tmax	Coord.	BA
130				
Right Middle Occipital Gyrus	3229	97.50	38 − 84 6	19
Left Middle Occipital Gyrus	3092	82.44	-36 − 86 6	19
100				
Cerebellar Vermis	1270	192.57	2 − 42 4	29
129				
Cerebellar Vermis	1448	140.21	6 − 56 0	
38				
Left Precuneus	3174	79.17	0 − 66 58	7
Right Superior Frontal Gyrus	241	32.07	30 4 60	6
37				
Left Posterior Cingulate Cortex	2019	141.39	0 − 54 30	31
Left Angular Gyrus	509	45.23	-52 − 68 28	39
27				
Right Middle Cingulate Cortex	2693	88.57	-4 − 24 28	23
Left Inferior Parietal Lobule	207	35.50	-36 − 62 48	7
Default-Mode Networks				
123				
Right Anterior Cingulate Cortex	4398	118.94	2 42 10	32
Right Insula Lobe	538	59.55	36 18 − 12	47
49				
Left Mid Orbital Gyrus	2941	115.46	0 48 − 6	10
Left Middle Temporal Gyrus	253	39.78	-58 − 14 − 18	21
90				
Left Angular Gyrus	2579	91.98	-52 − 62 30	39
Left Middle Frontal Gyrus	2269	52.91	-42 18 46	8
101				
Right Middle Frontal Gyrus	2450	57.54	30 18 54	8
Right Inferior Parietal Lobule	1892	99.84	54 − 56 40	40
Cognitive Control Networks				
83				
Left Middle Temporal Gyrus	2105	93.39	-46 6 − 30	21
Right Medial Temporal Pole	1588	96.98	48 10 − 26	21
114				
Left Superior Medial Gyrus	3955	103.29	0 60 22	10
Left Temporal Pole	733	40.71	-36 22 − 20	47
63				
Right Middle Frontal Gyrus	6987	115.49	32 58 4	10
Right Inferior Parietal Lobule	72	26.70	50 − 50 48	40
48				
Left Superior Medial Gyrus	2744	86.68	0 66 18	10
Right Cerebellum	77	31.19	48 − 72 − 38	
120				
L. Inf. Front. G. (p. Triangularis)	4236	91.65	-48 30 18	46
R. Inf. Front. G. (p. Triangularis)	855	52.20	50 22 28	46
146				
R. Inf. Front. G. (p. Opercularis)	7279	114.14	50 18 6	45
Left Insula Lobe	590	46.17	-34 24 − 2	13
119				
Left Insula Lobe	2186	116.66	-40 18 − 6	47
Right Insula Lobe	1381	88.71	44 16 − 2	47
96				
Left Inferior Parietal Lobule	3989	78.25	-24 − 72 46	7
Left Precentral Gyrus	711	47.22	-52 10 34	9
102				
Right Inferior Parietal Lobule	3397	82.40	44 − 42 48	40
R. Inf. Front, G. (p. Opercularis)	1660	51.33	54 12 30	9
133				
Right Rolandic Operculum	2745	102.29	54 4 4	22
Left Rolandic Operculum	766	51.31	-54 0 4	22
55				
Right Superior Parietal Lobule	3916	71.19	18 − 54 66	7
Right Cerebellum	106	33.04	26 − 44 − 48	
136				
Left Angular Gyrus	6603	74.10	-52 − 78 28	39
Right Middle Occipital Gyrus	807	58.53	44 − 78 34	19
Cerebellar Networks				
84				
Right Cerebellum	4173	150.37	30 − 68 − 38	
110				
Left Cerebellum	3906	126.64	-30 − 66 − 38	

detrended the time-courses to mitigate low frequency artifacts such as gradient heating. To estimate the spectral density, we utilized a sliding window approach (window size of 512) with a multi-taper frequency domain transfer and shifted one TR at each slide. Each windowed time course was demeaned and normalized to unit power. Later, each window was transferred to the frequency domain using multi-taper spectral estimation as implemented in GIFT. Finally, the estimated power spectra were averaged over each window.

2.6. Statistical analysis

We conducted statistical analysis with t-tests and corrected all statistical tests with 0.05 false discovery rate (FDR) using the Benjamini–Hochberg procedure (Benjamini et al., 1995). We tested the longitudinal differences with paired t-tests for EO and EC cases separately. We compared frequencies greater than 0.01 Hz and lower than 0.15 Hz, as this is a widely used spectral range of interest in fMRI studies. Before the statistical tests, motion as MFD and site were regressed out from the estimated spectral density. We compared EO and EC differences in the first timepoint and the second timepoint scans

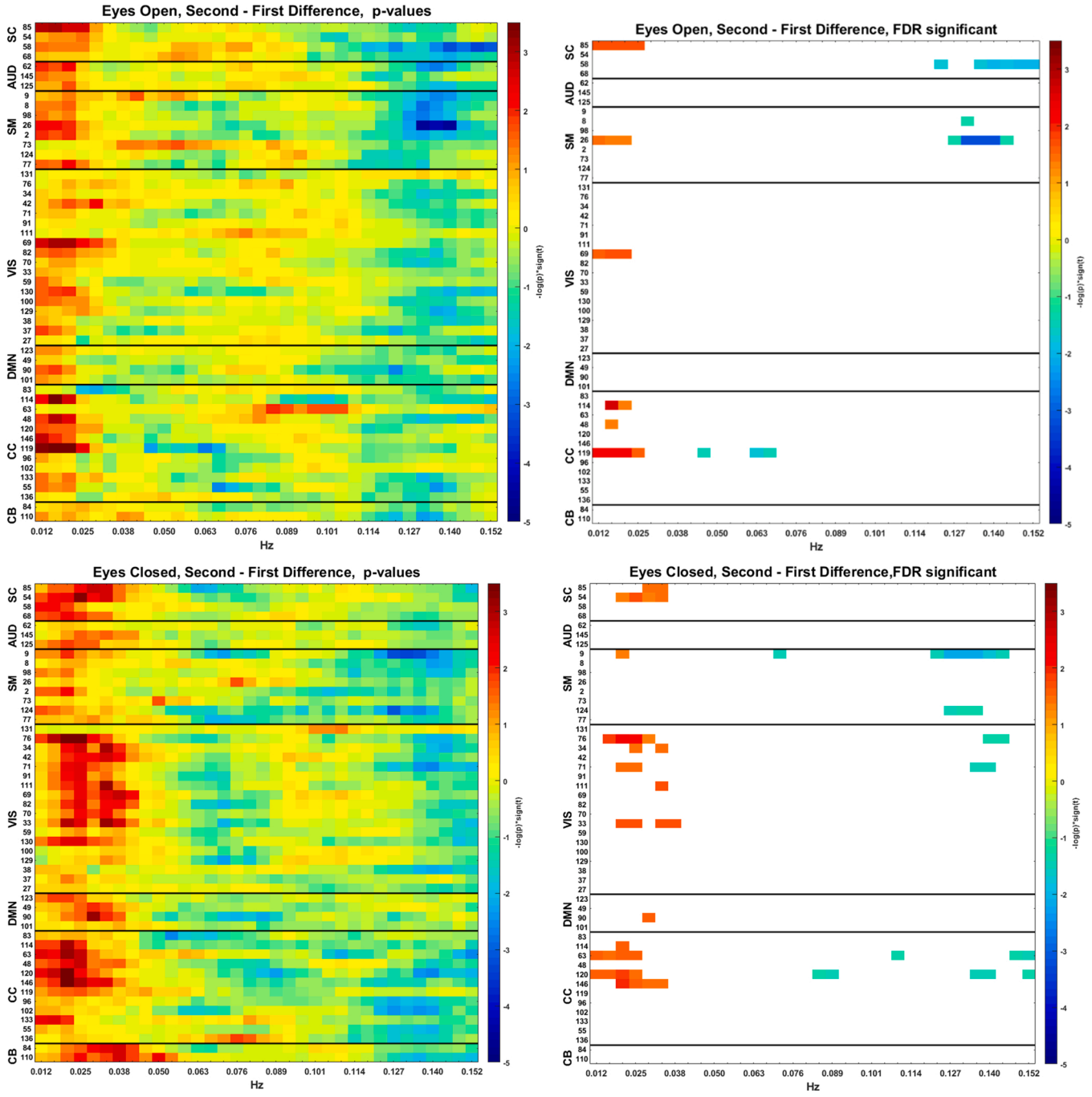

Fig. 2. The power spectral difference between second and first time points is displayed for EO and EC cases separately, where x direction shows the frequencies and y axis shows the different components. EO analysis includes 120 participants, EC analysis includes 115 participants. On the right, the results are displayed after FDR correction. There is an increase of power in low frequencies with development and a decrease of power in higher frequencies. There are significant differences especially in visual and cognitive control networks.

using paired t-test (111 subjects have both data available).

We also evaluated the differences in the longitudinal change in EO versus EC via a paired t-test and also examined sex differences between females and males in spectral power using two-sample t-tests in both first and second time point scans. The difference in development between females and males were analyzed using a two-sample t-test. Finally, we repeated the longitudinal spectral analysis on the ABDC dataset (Casey et al., 2018), collected as EO condition. For the statistical analysis, the FDR correction was applied at the network level for all DevCoG analyses. In this study, we used a relatively large gICA model order of 150, which resulted in 51 RSNs, and we evaluated a wide range of frequencies (34 frequency bins) rather than comparing summation of intervals. Importantly, the replication study revealed a consistent general pattern regardless of the threshold. For the ABCD dataset, the FDR correction was carried out across all networks and did reveal similar results comparing to those with FDR corrected at network level.

3. Results

3.1. Longitudinal spectral power differences

Spectral changes with development are presented in Fig. 2. Both EO and EC differences show a similar pattern, in which lower frequency power increases with age and higher frequency power decreases with

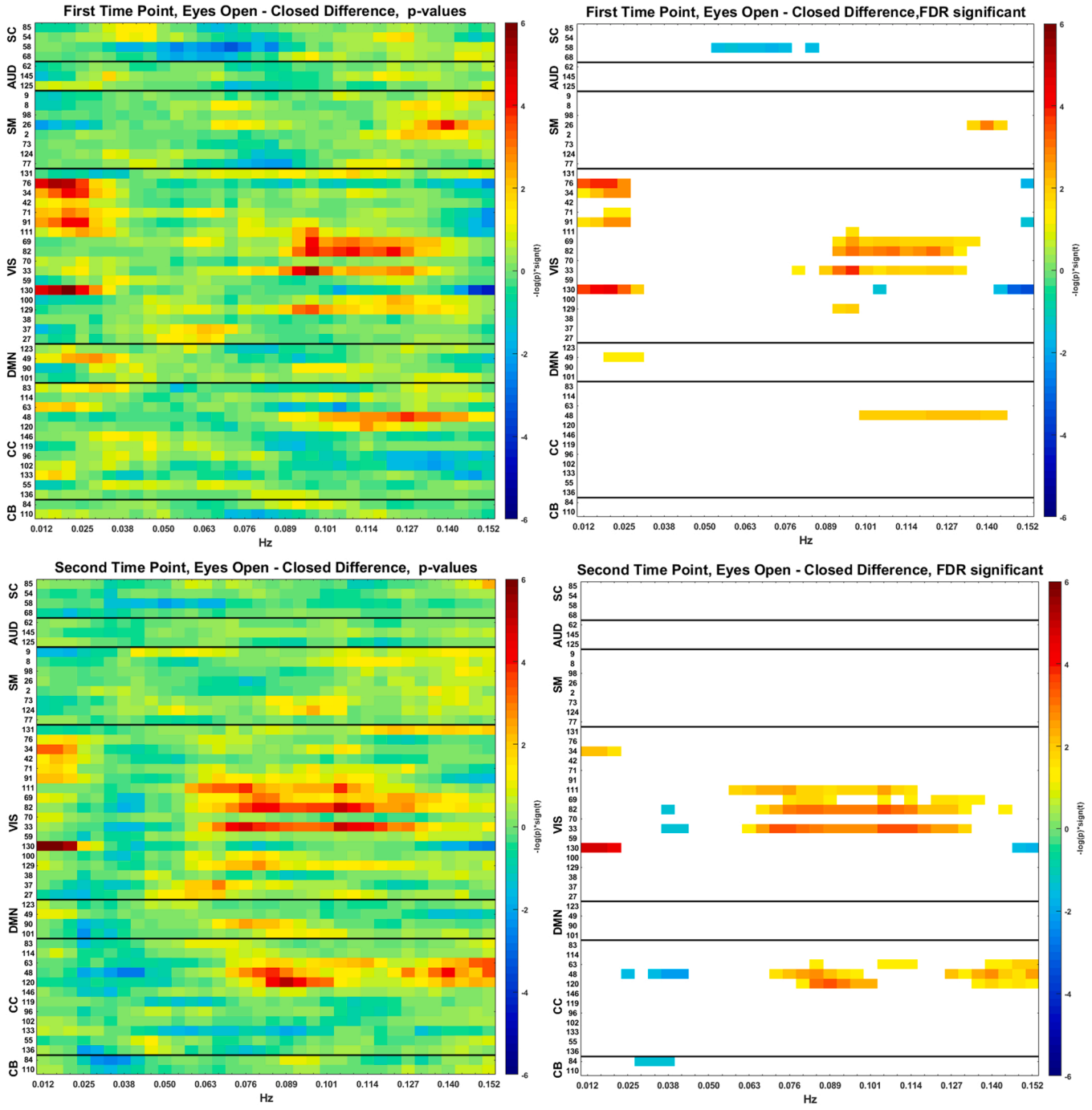

Fig. 3. Comparing Eyes open vs. Eyes Closed differences in power spectra in the first and second time point. There are significant differences in both time points mainly in Visual and cognitive control networks. 111 participants who had both EO, EC data available on multiple time points were included in this analysis.

age. Differences are more extensive for the EC case with more FDR significant regions. SC 58 and SM 8, 26 show FDR significant differences in higher frequencies for the EO case indicating power decreases as the individuals age. SC 85, SM 26, VIS 69 and CC 114, 48 and 119 have increasing power in low frequencies with age for the EO case. CC 119 has decreasing power with age in middle frequencies. Visual and cognitive control networks show the most FDR significant differences in the EC case. SC 85 and 54, SM 9, VIS 76, 34, 71, 111 and 33, DMN 90, CC 114, 63, 120 and 146 shows FDR significant increases in power in low frequencies. Some networks, SM 9 and 124, VIS 76 and 71, CC 63 and 120, have significant decrease in power in high frequencies as individuals age. SM 9 and CC 120 also have decreasing power in middle frequencies as individuals age.

3.2. Spectral differences between resting state condition

One-sample t-test results are presented in Fig. 3, showing EO and EC differences in power spectra in both first and second timepoints. We find significant differences in both first and second timepoint, mainly in visual networks and cognitive control networks. There are some significant differences in first timepoint in the SC networks, SM networks and DMN, that are not presented in second time point differences. CC and VIS network differences are more elaborated in the second time point. Fig. 4 shows the differences in power spectra over development between EO and EC cases. While significant differences are identified in only one CC 63, the un-thresholded t-values are highly structured, showing a pattern of low frequency power increases (with more in the EC case) and mid and high frequency increases (with more in the EO case) as individuals age.

The t-test results showing the longitudinal differences in the ABCD study are presented in Fig. 8. Comparing the un-thresholded ABCD results with those in the DevCoG EO data, the general pattern of increased power in low frequencies and decreased power in high frequencies can also be observed in the ABCD sample. There are some differences in the subnetworks, while the power increase in low frequencies was more consistent in the DevCoG case, in the ABCD study, SC networks do not have this increase in the very low frequencies, but they rather have it on the middle frequencies. Also, CB networks in the ABCD case show a decrease in power almost all frequencies. On the other hand, decrease in power in high frequencies are more consistent throughout the subnetworks in the ABCD case comparing to the DevCoG case. The ABCD results have more FDR significant regions compared to DevCoG, this can be expected considering the huge differences in sample size. Please note that the FDR comparison was carried out including all networks in the ABCD case, and the ABCD study uses a different ICA decomposition.

3.3. Spectral differences between sexes

Results showed significant spectral power differences between sexes at both time points. Sex differences at the first time point are displayed in Fig. 5; some SC and one VIS network have more power in middle frequencies, some SM, DMN and CC networks have more power in high frequencies in females comparing to males. VIS 100 shows more power in males in high frequencies. There are not many significant differences in low frequency power. The second time point differences are displayed in Fig. 6. At the second time point, the differences between sexes are enhanced, almost all networks have significantly more power in females in middle and high frequencies, while SM and CB networks have more power in boys in low frequencies. Fig. 7 shows the results of how the spectral power differences between sexes are changing with development. The differences are increasing with development, though statistically limited in one SM, one VIS, one DMN and one CC network.

4. Discussion

In this study, we investigated developmental changes in power spectra of rs-fMRI TCs assessed with gICA in a large longitudinal dataset (N = 124) focusing on children, where rapid developments occur. We found a significant increase in low frequency power and decrease in high frequency power in multiple networks with increasing age in EO and EC

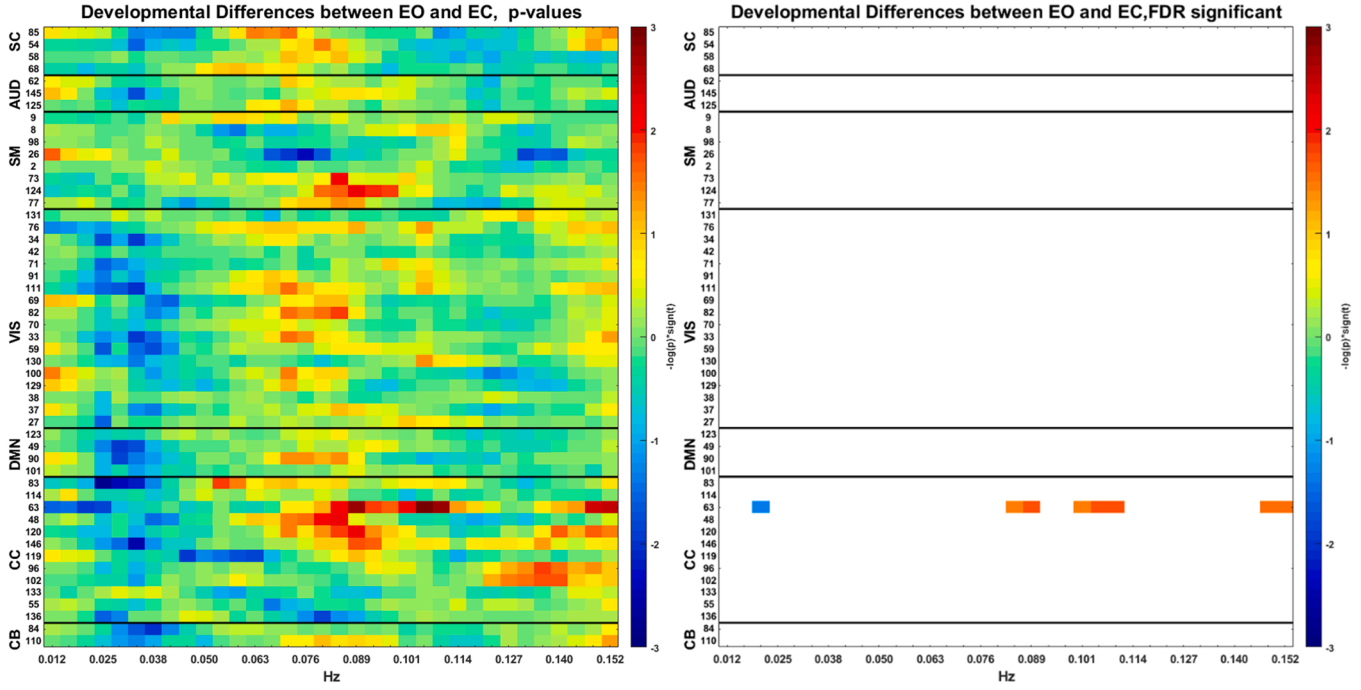

Fig. 4. Comparing developmental differences between (EO_second – EO_first difference) and (EC_second – EC_first difference). This shows the power spectra differences with development between the EO and EC cases. Though, significant results are limited, there is a structure in the p-values. Age-related differences are greater in low frequencies in EC case while developmental differences are greater in middle and high frequencies in EO case. 111 participants who had both EO, EC data available on multiple time points were included in this analysis.

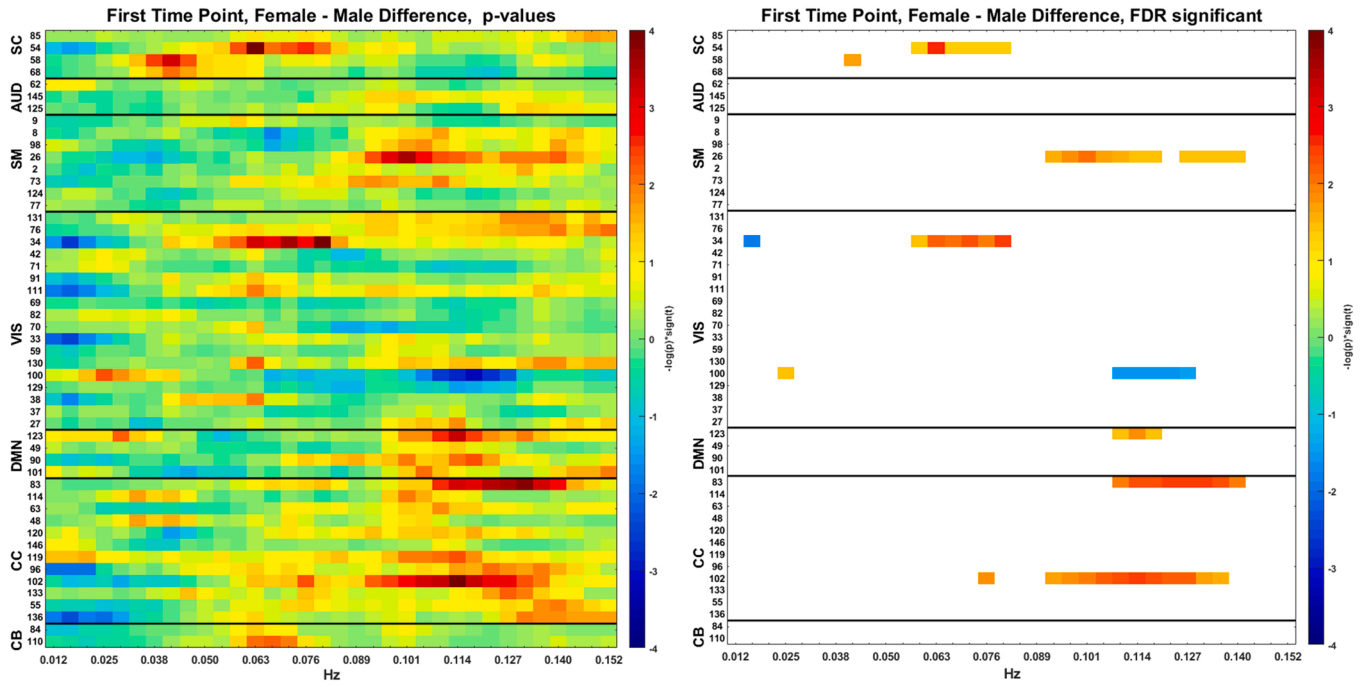

Fig. 5. Sex differences in spectral power at the first time point, in general middle and higher frequencies have more power in females except VIS #100. 113 females and 122 males were included in this analysis.

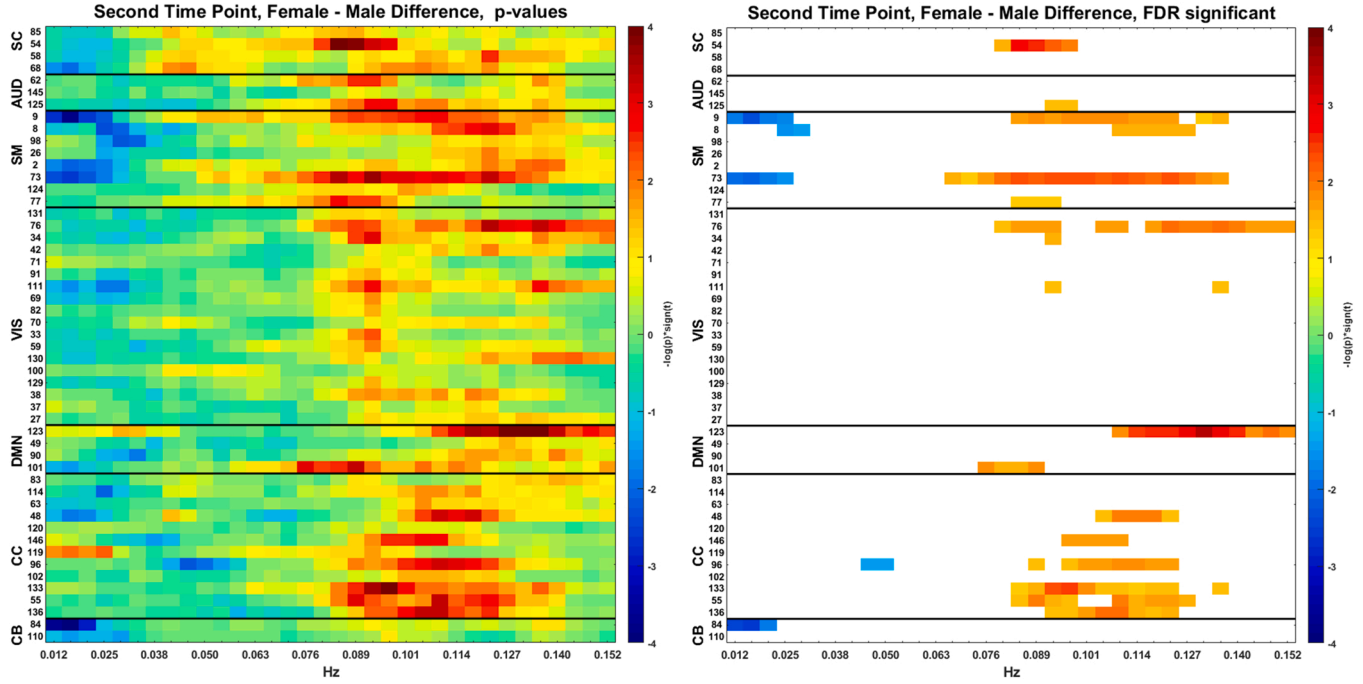

Fig. 6. Sex differences in spectral power at the second time point, middle and high frequencies have significantly more power in females in almost all networks, while males have more power in low frequencies in SM, CB and one CC network. There are more significant differences in the second time point compared to the first time point. 113 females and 122 males were included in this analysis.

scans. Our results indicated that power at low frequencies may be a general marker of typical brain development, as it was found in two dataset of healthy children in the current study and past studies have linked increased high-frequency power to schizophrenia and other clinical populations (Calhoun et al., 2011; Fu et al., 2018; Turner et al., 2013; Wang et al., 2016; Zang et al., 2007). We replicated our results using an independent dataset as well.

Our findings are consistent with some cross-sectional studies, though Allen et al. (2011) found a global decrease in low frequency power with increasing age across all RSNs in their study using a dataset containing 603 healthy subjects aged 12–71, they found that this trend was non-linear and for some RSNs, consistent with our study, the power stayed constant between roughly 12–15 years-old with even a small increase, and then decrease starts roughly after 15–16 years of age. They interpreted that these changes may have been due to gray matter concentration changes and other factors such as vascular compliance,

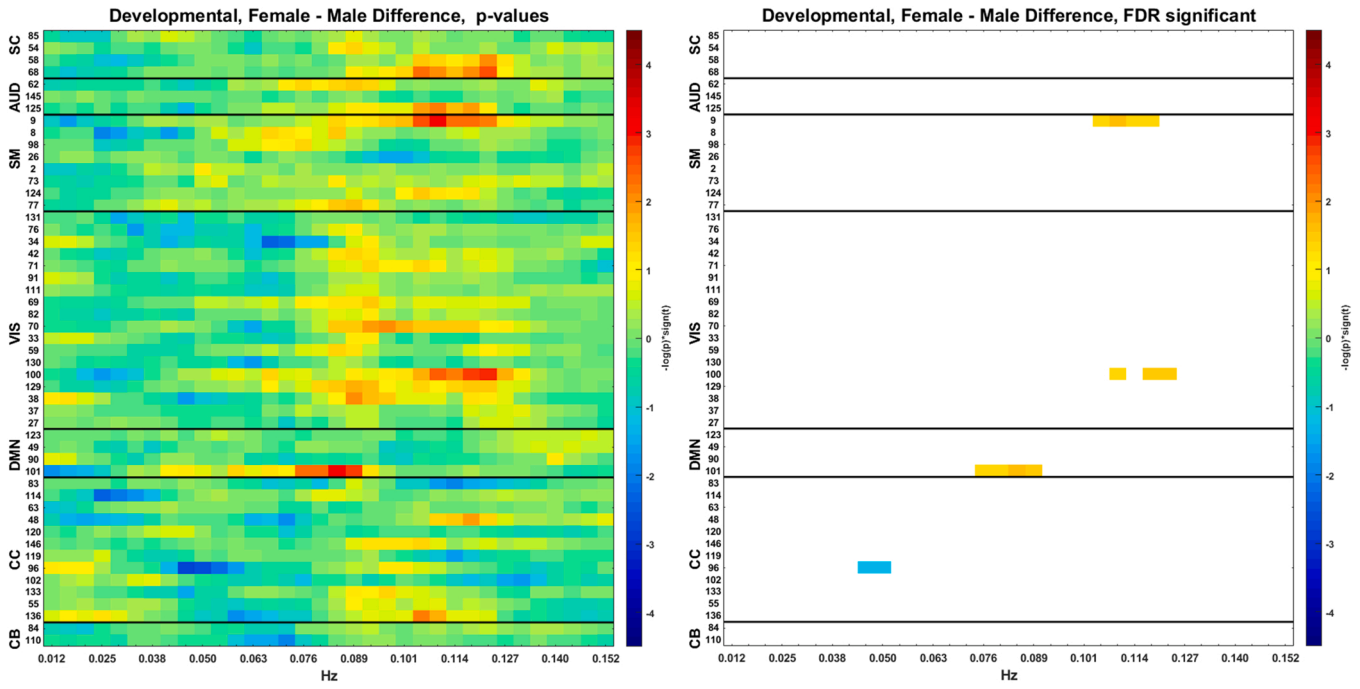

Fig. 7. Spectral power differences between sexes are increasing with development, though statistically limited. Females have more changes in power in middle-high frequencies. 113 females and 122 males were included in this analysis.

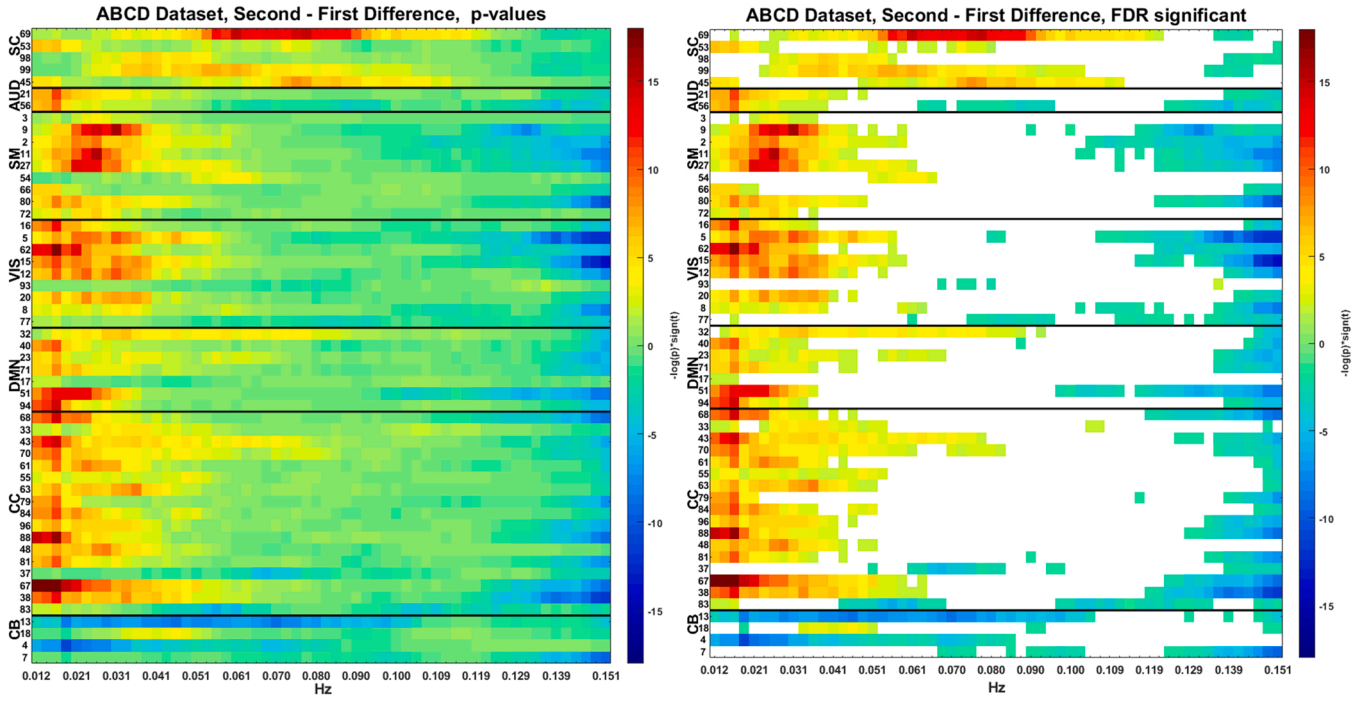

Fig. 8. Longitudinal power spectra differences on the ABCD dataset (3371 subjects). Results are consistent with those in Dev-CoG dataset (Fig. 2) and mostly replicated with power increasing in the lower frequencies and decreasing in the higher frequencies as individuals age.

degree of neural activation, and levels of basal activity. Consistently, (Agcaoglu et al., 2016), using a 4D spectral-temporal framework on the same dataset, also reported significant age-related decrease in low temporal frequencies between 0.01 and 0.15 Hz and significant increase in power after between 0.2 and 0.25 Hz in both hemispheres; and speculated that it may be related to an increase in reaction time. Our current study does not fully overlap in age with these existing studies, and our finding of increased power in low frequencies and decreased power in higher frequencies with development in early ages is consistent with prior non-linear age effects.

The focus of this study is the frequency interval between 0.01.01 Hz and 0.15 Hz. Studies showed that though fMRI signal from 0.01 to 0.073 Hz often related to the spontaneous activities in gray matter, 0.073–0.25 Hz activity is often detected in the white matter (Zhou et al., 2020). In our results, all the frequency bands that show an increase in power in the second time point are between 0.01 and 0.073 Hz interval

for both EO and EC cases. Also, we see reduced power in the second time point typically at frequencies from 0.073 to 0.15 Hz interval, with the only exception to this being CC 119 for the EO cases from 0.04 to 0.073 Hz. Bray (2017) found significant decreases in the global component of gray matter volume with increasing age in their cross-sectional study including 59 children aged 7–18 as well as trend level decreases in the global component of cerebral blood flow, and interestingly they did not find any significant age association in the global component of fALFF values (0.01–0.08 Hz). Although, this may imply the effect is mainly related to gray matter and white matter differences, we excluded the white matter components while selecting the RSNs.

We found significant EO and EC differences, and our results mainly suggest more spectral power changes in visual network and cognitive control in the EO case compared to EC case, but there are some networks that show more power in the EC case as well. Yang et al. (2007) investigated EO and EC differences in ALFF and found consistent results to our study; increased ALFF in bilateral visual cortex for the EO case. Yang et al. (2007) also reported significantly lower ALFF in right paracentral lobule in EO case. We found significant longitudinal effects between EO-EC differences in one network CC 63. Though, changes were relatively limited, un-thresholded results present an interesting pattern, suggesting lower frequency power increases more with age in EC case and middle and high frequency power increases more in EO case. A further study with a larger cohort may be needed to fully clarify this. Another interesting finding of our study is that we found more FDR significant differences in the EC case compared to the EO case. In Agcaoglu et al. (2019), we examined a subset of this dataset in a cross-sectional functional network connectivity framework and found more significant association with age, sex and social scores in EO case compared to the EC case. In this study we found some frequencies have higher spectral power in EO case compared to EC. This suggests the correlation differences in functional network connectivity in our previous studies may be related to the identified frequency differences. Sex differences mainly suggested that females have more power in high frequencies in almost all networks and males has more power in some SM and CB networks, and consistent with developmental results, these differences are more elaborated in the EC case.

We were able to replicate our main results of increase spectral power in low frequency and decrease spectral power in high frequency on an independent dataset. The second dataset revealed more FDR significant differences, which was expected considering the number of participants. It is important to note that the second dataset uses a different gICA decomposition and different model order, which can be interpreted as another strong evidence to the robustness of the findings.

Some limitations should be considered while interpreting the results. First, we have used a model order of 150 in the DevCog dataset and have used a model order of 100 in the ABCD dataset (NeuroMark template); the model order can have an influence on the network level results; examining the power spectra with lower and higher gICA model orders could also provide more insight on longitudinal spectral changes.

Secondly, (Klapwijk, Goddings et al., 2013; van Duijvenvoorde, Westhoff et al., 2019) reported altered connectivity with pubertal stage (independent of age) and (Kong, Hu et al., 2015) showed association between fALFF and subjective well-being; however, we did not have a measure of pubertal status for our participants and we did not include behavioral scores in our analysis. Based on these recent results, future developmental studies using our non-binning approach should include a pubertal scale to estimate pubertal stage in their participants. Furthermore, including behavioral measures will help future investigators interpret the effects of brain developmental changes on child development.

5. Conclusion

In sum, we investigated spectral power changes longitudinally in a pediatric sample for the first time and found significant increases in low frequency power and significant decreases in high frequency power with typical development; this finding was replicated using an independent dataset. This pattern can be interpreted as a general marker of typical development in children. Furthermore, we found that though both EO and EC resting state conditions can detect these markers, EC provides more elaborated differences. Spectral power was also significantly different between sexes, with high frequencies showing more spectral power in females compared to males.

CRediT authorship contribution statement

Oktay Agcaoglu: Performed gICA, visual classification of the components, spectral calculation and statistical analysis, prepared manuscripts, constructed figures. **Tony W. Wilson, Yu-Ping Wang, Julia M. Stephen:** Part of the group collected and provided DevCoG neuroimaging data and demographic information, principal investigators in the DevCoG Study, edited manuscript. **Zening Fu:** Provided ABCD neuroimaging data and their time-courses and edited manuscript. **Vince D. Calhoun:** Provided supervision in designing and implementing the analysis, Preparing the manuscription, provided funding, was also part of the group that collected and provided DevCoG neuroimaging data and demographic information; and one of principle investigators in the DevCog Study, edited manuscript.

Declaration of interest

Authors declare no conflict of interests.

Acknowledgment

This work was supported in part by National Institutes of Health grants R01MH121101 and R01EB020407, and NSF grants 1539067 and 2112455.

References

Agcaoglu, O., Miller, R., Mayer, A.R., Hugdahl, K., Calhoun, V.D., 2016. Increased spatial granularity of left brain activation and unique age/gender signatures: a 4D frequency domain approach to cerebral lateralization at rest. Brain Imaging Behav. 10 (4), 1004–1014. https://doi.org/10.1007/s11682-015-9463-8. ⟨http://www.ncbi.nlm.nih.gov/pubmed/26489978⟩.

Agcaoglu, O., Wilson, T.W., Wang, Y.P., Stephen, J., Calhoun, V.D., 2019. Resting state connectivity differences in eyes open versus eyes closed conditions. Hum. Brain Mapp. 40 (8), 2488–2498. https://doi.org/10.1002/hbm.24539. ⟨https://www.ncbi.nlm.nih.gov/pubmed/30720907⟩.

Agcaoglu, O., Wilson, T.W., Wang, Y.P., Stephen, J.M., Calhoun, V.D., 2020. Dynamic resting-state connectivity differences in eyes open versus eyes closed conditions. Brain Connect 10 (9), 504–519. https://doi.org/10.1089/brain.2020.0768. ⟨https://www.ncbi.nlm.nih.gov/pubmed/32892633⟩.

Allen, E.A., Erhardt, E.B., Damaraju, E., Gruner, W., Segall, J.M., Silva, R.F., Calhoun, V. D., 2011. A baseline for the multivariate comparison of resting-state networks. Front Syst. Neurosci. 5, 2. https://doi.org/10.3389/fnsys.2011.00002. ⟨http://www.ncbi.nlm.nih.gov/pubmed/21442040⟩.

Benjamini, Y., Hochberg, Y., 1995. Controlling the false discovery rate - a practical and powerful approach to multiple testing. J. R. Stat. Soc. Ser. B-Stat. Methodol. 57 (1), 289–300. https://doi.org/10.1111/j.2517-6161.1995.tb02031.x.

Biswal, B., Yetkin, F.Z., Haughton, V.M., Hyde, J.S., 1995. Functional connectivity in the motor cortex of resting human brain using echo-planar MRI. Magn. Reson Med 34 (4), 537–541. ⟨http://www.ncbi.nlm.nih.gov/pubmed/8524021⟩.

Bray, S., 2017. Age-associated patterns in gray matter volume, cerebral perfusion and BOLD oscillations in children and adolescents. Hum. Brain Mapp. 38 (5), 2398–2407. https://doi.org/10.1002/hbm.23526. ⟨https://www.ncbi.nlm.nih.gov/pubmed/28117505⟩.

Calhoun, V.D., Sui, J., Kiehl, K., Turner, J., Allen, E., Pearlson, G., 2011. Exploring the psychosis functional connectome: aberrant intrinsic networks in schizophrenia and bipolar disorder. Front Psychiatry 2, 75. https://doi.org/10.3389/fpsyt.2011.00075. ⟨https://www.ncbi.nlm.nih.gov/pubmed/22291663⟩.

Casey, B.J., Cannonier, T., Conley, M.I., Cohen, A.O., Barch, D.M., Heitzeg, M.M., Workgroup, A.I.A., 2018. The adolescent brain cognitive development (ABCD) study: imaging acquisition across 21 sites. Dev. Cogn. Neurosci. 32, 43–54. https://doi.org/10.1016/j.dcn.2018.03.001. ⟨https://www.ncbi.nlm.nih.gov/pubmed/29567376⟩.

Du, Y., Fan, Y., 2013. Group information guided ICA for fMRI data analysis. Neuroimage 69, 157–197. https://doi.org/10.1016/j.neuroimage.2012.11.008.

Du, Y., Allen, E.A., He, H., Sui, J., Wu, L., Calhoun, V.D., 2016. Artifact removal in the context of group ICA: A comparison of single-subject and group approaches. Hum Brain Mapp 37 (3), 1005–1025. https://doi.org/10.1002/hbm.23086.

Du, Y., Fu, Z., Sui, J., Gao, S., Xing, Y., Lin, D., Alzheimer's, Disease Neuroimaging, I., 2020. NeuroMark: An automated and adaptive ICA based pipeline to identify reproducible fMRI markers of brain disorders. Neuroimage Clin. 28, 102375 https://doi.org/10.1016/j.nicl.2020.102375. ⟨https://www.ncbi.nlm.nih.gov/pubmed/32961402⟩.

van Duijvenvoorde, A.C.K., Westhoff, B., de Vos, F., Wierenga, L.M., Crone, E.A., 2019. A three-wave longitudinal study of subcortical-cortical resting-state connectivity in adolescence: Testing age- and puberty-related changes. Hum. Brain Mapp. 40 (13), 3769–3783. https://doi.org/10.1002/hbm.24630. ⟨https://www.ncbi.nlm.nih.gov/pubmed/31099959⟩.

Egorova, N., Veldsman, M., Cumming, T., Brodtmann, A., 2017. Fractional amplitude of low-frequency fluctuations (fALFF) in post-stroke depression. Neuroimage Clin. 16, 116–124. https://doi.org/10.1016/j.nicl.2017.07.014. ⟨https://www.ncbi.nlm.nih.gov/pubmed/28794972⟩.

Fu, Z., Tu, Y., Di, X., Du, Y., Pearlson, G.D., Turner, J.A., Calhoun, V.D., 2018. Characterizing dynamic amplitude of low-frequency fluctuation and its relationship with dynamic functional connectivity: An application to schizophrenia. Neuroimage 180 (Pt B), 619–631. https://doi.org/10.1016/j.neuroimage.2017.09.035.

Garrity, A.G., Pearlson, G.D., McKiernan, K., Lloyd, D., Kiehl, K.A., Calhoun, V.D., 2007. Aberrant "default mode" functional connectivity in schizophrenia. Am. J. Psychiatry, 164 (3), 450–457. https://doi.org/10.1176/ajp.2007.164.3.450. ⟨https://www.ncbi.nlm.nih.gov/pubmed/17329470⟩.

Jernigan, T.L., Brown, S.A., Dowling, G.J., 2018. The Adolescent Brain Cognitive Development Study. J. Res Adolesc. 28 (1), 154–156. https://doi.org/10.1111/jora.12374. ⟨https://www.ncbi.nlm.nih.gov/pubmed/29460352⟩.

Klapwijk, E.T., Goddings, A.L., Burnett Heyes, S., Bird, G., Viner, R.M., Blakemore, S.J., 2013. Increased functional connectivity with puberty in the mentalising network involved in social emotion processing. Horm. Behav. 64 (2), 314–322. https://doi.org/10.1016/j.yhbeh.2013.03.012. ⟨https://www.ncbi.nlm.nih.gov/pubmed/23998674⟩.

Kong, F., Hu, S., Wang, X., Song, Y., Liu, J., 2015. Neural correlates of the happy life: the amplitude of spontaneous low frequency fluctuations predicts subjective well-being. Neuroimage 107, 136–145. https://doi.org/10.1016/j.neuroimage.2014.11.033. ⟨https://www.ncbi.nlm.nih.gov/pubmed/25463465⟩.

Miller, R.L., Erhardt, E.B., Agcaoglu, O., Allen, E.A., Michael, A.M., Turner, J.A., Calhoun, V.D., 2015. Multidimensional frequency domain analysis of full-volume fMRI reveals significant effects of age, gender, and mental illness on the spatiotemporal organization of resting-state brain activity. Front Neurosci. 9, 203. https://doi.org/10.3389/fnins.2015.00203. ⟨https://www.ncbi.nlm.nih.gov/pubmed/26136646⟩.

Stephen, J.M., Solis, I., Janowich, J., Stern, M., Frenzel, M.R., Eastman, J.A., Calhoun, V. D., 2021. The Developmental Chronnecto-Genomics (Dev-CoG) study: A multimodal study on the developing brain. Neuroimage 225, 117438. https://doi.org/10.1016/j.neuroimage.2020.117438. ⟨https://www.ncbi.nlm.nih.gov/pubmed/33039623⟩.

Turner, J.A., Damaraju, E., van Erp, T.G., Mathalon, D.H., Ford, J.M., Voyvodic, J., Calhoun, V.D., 2013. A multi-site resting state fMRI study on the amplitude of low frequency fluctuations in schizophrenia. Front Neurosci. 7, 137. https://doi.org/10.3389/fnins.2013.00137. ⟨https://www.ncbi.nlm.nih.gov/pubmed/23964193⟩.

Wang, X.-H., Jiao, Y., Li, L., & Ding, Z. (2016). *Abnormal developmental trajectories of amplitude of low frequency fluctuations within intrinsic connectivity networks for school-age boys with ADHD*.

Yang, H., Long, X.Y., Yang, Y., Yan, H., Zhu, C.Z., Zhou, X.P., Gong, Q.Y., 2007. Amplitude of low frequency fluctuation within visual areas revealed by resting-state functional MRI. Neuroimage 36 (1), 144–152. https://doi.org/10.1016/j.neuroimage.2007.01.054. ⟨https://www.ncbi.nlm.nih.gov/pubmed/17434757⟩.

Zang, Y.F., He, Y., Zhu, C.Z., Cao, Q.J., Sui, M.Q., Liang, M., Wang, Y.F., 2007. Altered baseline brain activity in children with ADHD revealed by resting-state functional MRI. Brain Dev. 29 (2), 83–91. https://doi.org/10.1016/j.braindev.2006.07.002.

Zhan, J., Gao, L., Zhou, F., Bai, L., Kuang, H., He, L., Gong, H., 2016. Amplitude of low-frequency fluctuations in multiple-frequency bands in acute mild traumatic brain injury. Front Hum. Neurosci. 10, 27. https://doi.org/10.3389/fnhum.2016.00027. ⟨https://www.ncbi.nlm.nih.gov/pubmed/26869907⟩.

Zhou, J., Ma, X., Li, C., Liao, A., Yang, Z., Ren, H., Chen, X., 2020. Frequency-specific changes in the fractional amplitude of the low-frequency fluctuations in the default mode network in medication-free patients with bipolar II depression: a longitudinal functional MRI study. Front Psychiatry 11, 574819. https://doi.org/10.3389/fpsyt.2020.574819. ⟨https://www.ncbi.nlm.nih.gov/pubmed/33488415⟩.

Zou, Q.H., Zhu, C.Z., Yang, Y., Zuo, X.N., Long, X.Y., Cao, Q.J., Zang, Y.F., 2008. An improved approach to detection of amplitude of low-frequency fluctuation (ALFF) for resting-state fMRI: fractional ALFF. J. Neurosci. Methods 172 (1), 137–141. https://doi.org/10.1016/j.jneumeth.2008.04.012. ⟨https://www.ncbi.nlm.nih.gov/pubmed/18501969⟩.